THE SIGNIFICANCE OF PARTITION COEFFICIENTS OF HEAT PRODUCTION ELEMENTS IN THE LUNAR INTERIOR FOR DETERMINING THE PRESENT-DAY SELENOTHERM

A. Roy[1], A. Mallik[1], P. M. Bremner[2], H. F. Haviland[2], M. Diamond[3], T. J. Goepfert[4], and R. L. Hervig[4], [1]Department of Geosciences, University of Arizona, Tucson, AZ 85721, USA, [2]NASA Marshall Space Flight Center, Huntsville, AL 35805, USA, [3]Department of Physics, University of Illinois Chicago, Chicago, IL 60607, USA, [4]School of Earth and Space Exploration, Arizona State University, Tempe, AZ 85287, USA; arkadeeproy@arizona.edu

Introduction: The lunar thermal profile (the selenotherm) is key to understanding lunar volcanism, mantle mineralogy and petrology, mantle dynamics, and thermoelastic properties of the solid Moon. The range of selenotherms derived independently from geophysical inversions of seismic, gravity, and electromagnetic data span ~800 °C which is too large to apply petrogenesis models or perform geodynamic simulations [1].

The present-day selenotherm is primarily a function of the radiogenic heat generated in different layers in the interior of the Moon and their respective thermal properties. Other sources of early heat such as those generated from planetary accretion, mantle and core crystallization, or crystal compaction are considered negligible [e.g., 2]. This assumption is based on the fact that the small size of the Moon aids in quickly losing heat from these other sources. Controlling factors on the nature of the present-day selenotherm are the distribution of heat producing elements (HPEs: U, Th, and K), mineralogy of the different mantle stratigraphic horizons and their respective thermal conductivities. As the lunar magma ocean crystallized, the HPEs which are incompatible in most lunar mantle minerals were accumulated in the last dregs of the lunar magma ocean (LMO). In addition to the HPEs, the final residual LMO was also highly enriched in Fe and Ti which crystallized the high density ilmenite-bearing cumulates (IBCs) hypothesized to be gravitationally unstable and result in mantle overturn [3]. We explored the role of overturn in perturbing the selenotherm as it is a potential mechanism in transporting significant quantities of radiogenic elements to an otherwise HPE-depleted lower mantle. To evaluate selenotherms for different overturn scenarios, we considered three models: no overturn, overturn of 50% of the IBCs, and complete overturn. However, the large degree of uncertainty in the HPE distribution of the lunar mantle and crust poses a major roadblock for constraining the selenotherm. We addressed this problem by providing partition coefficients (K_d) of HPEs relevant for the lunar interior. K_d is defined as the ratio of the concentration of an element in the mineral to the melt in equilibrium.

Methods: Piston-cylinder experiments were performed at the University of Arizona to determine K_d of HPEs for minerals crystallizing from the LMO. Experiments with plagioclase and pyroxene on the liquidus at 1200 – 1220 °C and 0.5 GPa were equilibrated for 48 hours. Graphite capsules were used to achieve low oxygen fugacity conditions relevant for the lunar interior. Major element phase compositions were analyzed using the CAMECA SX100 electron microprobe at the, University of Arizona. Trace U, Th and K were measured using the LA-ICPMS and Cameca SIMS facility at Arizona State University.

The solidification of the LMO was modeled by a step-by-step fractional crystallization on a 600-km deep LMO using the lunar mantle stratigraphic sequence determined by [4]. The lunar primitive upper mantle (LPUM) [5] composition was chosen as the Bulk Silicate Moon (or BSM) and was assumed to be equally distributed throughout the LMO column. We designate the final 2.5% of the residual LMO by mass as the IBCs. Thickness of the crust has been set to 40 km to reflect the average lunar crustal thickness as determined by GRAIL [6]. A 400 km radius of metallic core [7-9] and an undifferentiated lower mantle has been assumed beneath the 600 km deep LMO.

Since the Earth-Moon system has a common origin [10], we consider BSM equivalent to bulk silicate Earth (BSE) for trace elements like U and Th. K concentrations were calculated as K/U = 1244.2 for lunar materials to account for its volatile nature [11]. HPE concentrations in the core were calculated using the following partition coefficients: K_d^U (1.05×10^{-3} - 1.02×10^{-3}), K_d^{Th} (0.17 - 2.49) and K_d^K (0.39 - 10.55) from the literature [12,13]. Two different HPE concentrations for BSM were explored in our models:

1. McDonough and Sun (1995) BSE [14] :
   U = 20.3 ppb, Th = 79.5 ppb, K = 25.26 ppm
2. Faure et al. (2020) BSE [12]:
   U = 11.42 ppb, Th = 43.2 ppb, K = 14.21 ppm

K_d between glass, clinopyroxene, and plagioclase were determined for U, Th, and K from our experiments. Whereas minimum and maximum K_d reported in the literature [15-21] were used for olivine, orthopyroxene and quartz. Selenotherms are generated by incorporating the maximum and minimum HPE estimates of different mantle layers into a 1-D thermal conduction equation for a spherical shell model.

Results: Figure 1 shows the Onuma diagrams for plagioclase and augite at 1200°C and 1220°C from our experiments. In plagioclase (An_{95}) we note that HPEs are slightly more incompatible at higher temperatures. These well-correlated Onuma plots show that the experimental and analytical techniques used have produced robust data quality.

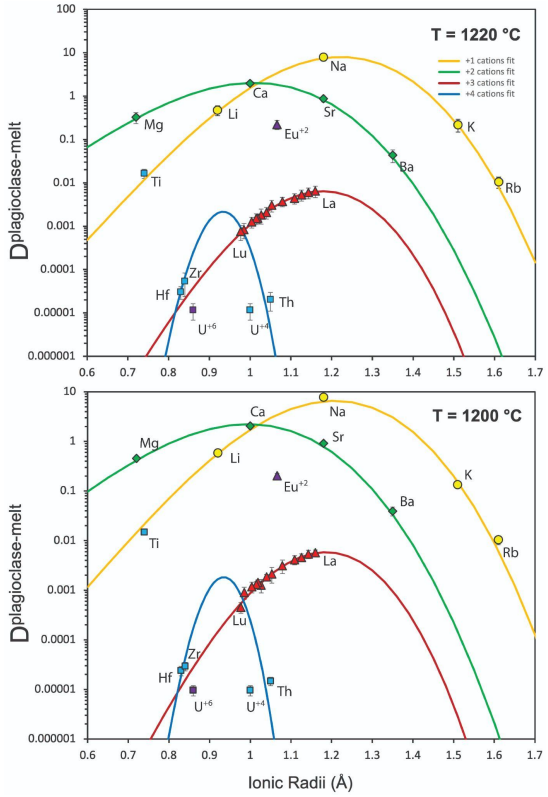

Figure 1. Onuma diagrams for plagioclase-melt at 1200°C and 1220°C, and 0.5 GPa.

Discussion: The HPEs are concentrated within the IBCs, seen in the shallow mantle in Figure 2, which is the final product of crystallization from the LMO. Consequently, radiogenic decay within the IBCs are the largest contributor to the present-day heat production in the lunar interior. We also note that the distribution of HPE concentrations derived from McDonough and Sun (1995) [14] are often more than an order of magnitude higher than the BSE derived from the bulk composition reported by Faure et al. (2020) [12]. Therefore, the models based upon McDonough and Sun (1995) [14] yield significantly hotter selenotherms. Figure 2. shows the overlapping of HPE abundances calculated from both studies [12,14] in certain sections of the lunar mantle. This overlap is the result of uncertainty in K_d^{HPEs} highlighting the importance of experimentally constraining these partition coefficients.

100% efficient overturning of the IBCs and foundering at the core-mantle boundary would lead to considerable warming of the core. In contrast, a no-overturn scenario results in preferential heating of the upper mantle. We report selenotherms for both these end member scenarios along with the intermediate scenario with 50% overturn.

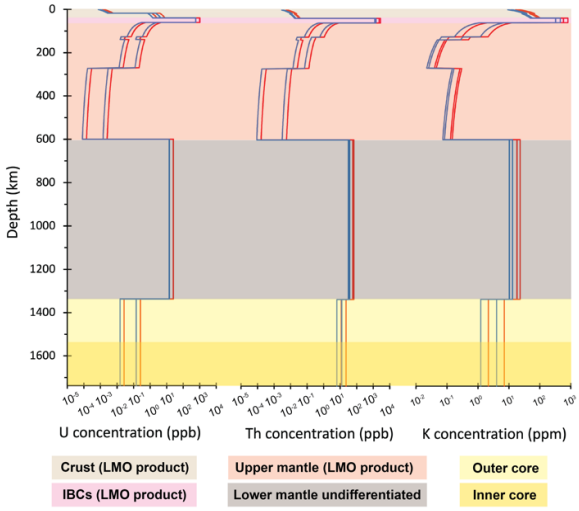

Figure 2. Present-day distribution of HPEs within the lunar interior. Red and blue lines represent modeling of McDonough and Sun (1995) [14] and Faure et al. (2020) [12] initial BSM, respecively. Upper and lower bounds represent maximum and minimum K_d. The internal layers in the Moon are labeled. The 600 km LMO crystallizes [4] to form the crust and upper mantle.

References: [1] Bremner P.M. et al. (2021) *LPI Contrib*, 2635, 5052. [2] Siegler M. et al. (2022) *JGR: Planets*, 127, e2022JE007182. [3] Elkins-Tanton et al. (2002) *EPSL*, 196, 239-249 [4] Charlier B. et al. (2018a) *Geochim Cosmochim Acta*, 234, 50–69. [5] Longhi J. (2006) *Geochim Cosmochim Acta*, 70, 5919–5934. [6] Wieczorek M.A. et al. (2012) *Science* 339, 671-675. [7] Weber R.C. et al. (2011) *Science*, 331, 309-312. [8] Garcia R.F. et al. (2011) *Phys. Earth Planet. Inter*, 188, 96-113. [9] Hood L.L. et al (1999) *Geophys. Res. Lett*, 26, 2327-2330. [10] Canup R. (2012) *Science* 338, 1052-1055 [11] Korotev R.L. (1998) *JGR: Planets*, *103*, 1691–1701. [12] Faure P. et al. (2020) *Geochim Cosmochim Acta*, 275, 83-98. [13] Steenstra E.S. et al. (2018) *Sci. Rep*, 8, 7053. [14] McDonough W.F. & Sun S.-s. (1995) *Chem. Geol*, 120, 223-253. [15] Nash W.P. & Crecraft H.R. (1985) *Geochim Cosmochim Acta*, 49, 2309-2322. [16] Salters V.J.M. & Longh J (1999) *EPSL*, 166, 15-30. [17] Beattie P. (1993) *Nature*, 363, 63–65. [18] McKenzie D. & O'nions R.K. (1991) *J. Petrol*, 32, 1021-1091. [19] Kelemen P.B. et al. (1993) *EPSL*, 120, 111-134. [20] Onuma N. et al. (1968) *EPSL*, 5, 47-51. [21] Philpotts J.A. & Schnetzler C.C. (1970) *Geochim Cosmochim Acta*, 34, 307-322.